Available online at www.sciencedirect.com
ScienceDirect
International Journal of Heat and Mass Transfer 50 (2007) 1750–1761
International Journal of HEAT and MASS TRANSFER
www.elsevier.com/locate/ijhmt

Estimation of heat transfer coefficient on the fin of annular-finned tube heat exchangers in natural convection for various fin spacings

Han-Taw Chen *, Wei-Lun Hsu

Department of Mechanical Engineering, National Cheng Kung University, Tainan 701, Taiwan

Received 15 May 2006; received in revised form 13 October 2006
Available online 22 December 2006

Abstract

The finite difference method in conjunction with the least-squares scheme and experimental temperature data is used to predict the average heat transfer coefficient and fin efficiency on the fin of annular-finned tube heat exchangers in natural convection for various fin spacings. The radiation and convection heat transfer coefficients are simultaneously taken into consideration in the present study. The heat transfer coefficient on this annular circular fin is assumed to be non-uniform. Thus the whole annular circular fin is divided into several sub-fin regions in order to predict the average heat transfer coefficient $\overline{h}$ and fin efficiency from the knowledge of the ambient temperature, tube temperature and fin temperature recordings at several selected measurement locations. The results show that the $\overline{h}$ value increases with increasing the fin spacing S, and the fin efficiency decreases with increasing the fin spacing S. However, these two values respectively approach their corresponding asymptotical values obtained from a single fin as $S \to \infty$. The fin temperature departs from the ideal isothermal situation and decreases more rapidly away from the circular center with increasing the fin spacing. In order to validate the accuracy of the present inverse scheme, a comparison of the average heat transfer coefficient on the fin between the present estimates and those obtained from the correlation recommended by current textbooks is made.

1. Introduction

Annular-finned tube heat exchangers are commonly used in industry. In designing such heat exchangers, it is necessary to note the interactions between the local heat transfer and flow distribution within the fins. The previous works about the effect of the fin spacing of annular-finned tube heat exchangers were limited to the experiments [1]. Thus the present study applies the hybrid inverse scheme in conjunction with experimental temperature data to estimate the heat-transfer characteristics of annular-finned tube heat exchangers. The fin in heat exchangers is always applied to increase the heat flow per unit of basic surface. The analysis of a continuous plate fin pierced by a regularly spaced array of circular tubes in staggered and in-line arrays has many engineering applications [2]. In order to simplify the problem considered, the calculation of the standard fin efficiency usually assumes that the heat transfer coefficient is constant over the plate fin. However, it is well known that there exists a very complex flow pattern within a plate finned-tube heat exchanger due to a plume of the heated air rising above the horizontal circular tube in natural convection. The boundary layer over a heated horizontal tube starts to develop at the bottom of the tube and increases in thickness along the circumference of the tube. The flow forms a low-velocity region above the tube. Thus the heat transfer coefficient is lowest on the top region of the tube. This causes local variations of the heat transfer coefficient on the fin. On the other hand, the heat transfer coefficient on the fin is non-uniform. These phenomena can be found from Refs. [3,4]. As shown in Ref. [5], the measurements of the local heat transfer coefficient on plain fins under steady-state heat transfer conditions were very difficult to perform, since the local fin temperature and local heat flux were required. Moreover, reliability is an

* Corresponding author. Fax: +886 6 235 2973.
E-mail address: htchen@mail.ncku.edu.tw (H.-T. Chen).

0017-9310/$ - see front matter © 2006 Elsevier Ltd. All rights reserved.
doi:10.1016/j.ijheatmasstransfer.2006.10.021

Nomenclature

A_f	area of the annular circular fin, m^2
A_j	area of the jth sub-fin region, m^2
$[A]$	global conduction matrix
$[F]$	force matrix
g	acceleration of gravity, m/s^2
h	local heat transfer coefficient, W/m^2 K
$\bar{h}$	unknown average heat transfer coefficient on the whole fin, W/m^2 K
$\bar{h}_j$	unknown average heat transfer coefficient on the jth sub-fin region, W/m^2 K
k	thermal conductivity of the fin, W/m K
k_{air}	thermal conductivity of the air, W/m K
ℓ_r	distance between two neighboring nodes in the r-direction, $\ell_r = (R_o - R_i)/(N_r - 1)$
ℓ_θ	distance between two neighboring nodes in the θ-direction, $\ell_\theta = 2\pi/(N_\theta - 1)$
N	number of sub-fin regions
Nu_s	Nusselt number defined in Eq. (33)
N_r	number of nodes in the r-direction
N_θ	number of nodes in the θ-direction
Q	total heat rate dissipated from the whole annular circular fin, W
q_j	heat rate dissipated from the jth sub-fin region, W
r	spatial coordinate
R_i	inner radius of the annular circular fin or outer radius of the circular tube, m
R_o	outer radius of the annular circular fin, m
Ra_s	Rayleigh number defined in Eq. (31)
S	fin spacing, m
T	fin temperature, K
T_j	measured temperature on the jth sub-fin region, K
T_o	outer surface temperature of the circular tube, K
T_∞	ambient temperature, K

Greek symbols

α	thermal diffusivity of the air, m^2/s
β	volumetric thermal expansion coefficient, 1/K
δ	fin thickness, m
η_f	fin efficiency
ν	kinematic viscosity of the air, m^2/s
θ	spatial coordinate
ω_j	limit of error of the thermocouple
ξ	ratio of R_o to R_i, R_o/R_i

Superscripts

cal	calculated value
mea	measured data

important concept in engineering design, and the use of reliable components enables the designers to utilize more sophisticated techniques to improve the performance [6]. Thus the estimation of a more accurate heat transfer coefficient on the fin is an important task for the device of the high-performance heat exchangers.

It is well known that the physical quantities and surface conditions of the test material can be predicted using the measured temperatures inside this material. Such problems are called the inverse heat conduction problems. These inverse problems have become an interesting subject recently. To date, various inverse methods in conjunction with the measured temperatures inside the test material have been developed for the analysis of the inverse heat conduction problems [7,8]. However, to the authors' knowledge, a few investigators performed the prediction of the local heat transfer coefficients on the annular circular fin inside the plate finned-tube heat exchangers.

Lin et al. [9] used the finite difference method in conjunction with the linear least-squares scheme to estimate the space-variable heat transfer coefficient on a heated cylinder normal to the laminar and turbulent air streams. Due to the requirement of the local fin temperature measurements, the estimations of the local heat transfer coefficients on the plate fin under steady-state heat transfer conditions are generally more difficult than those on the boundary surface of a physical geometry, as shown in Ref. [9]. Thus a few researchers predicted the distribution of the local heat transfer coefficients on a plate fin [3,4,10–12]. Saboya and Sparrow [10] and Rosman et al. [11] cast solid naphthalene plates in the form of a plate-fin-and-tube flow passage and used mass transfer techniques to infer the local heat transfer coefficient from the heat-mass transfer analogy. The local mass transfer coefficient was defined by measuring the thickness of naphthalene lost by sublimation during a timed test run. Recently, Ay et al. [12] performed an experimental study with the infrared thermovision to monitor the temperature distribution on a plate-fin surface inside the plate finned-tube heat exchangers and then the local heat transfer coefficient on the test fin can be determined using the obtained experimental temperature measurements. However, the fin efficiency on the fin inside the plate finned-tube heat exchangers was not shown in the work of Ay et al. [12]. Sometimes, it is maybe difficult to measure the temperature distributions on the fin of plate finned-tube heat exchangers using the infrared thermography and the thermocouples for some practical heat transfer problems. Park et al. [13] applied a commercial finite-volume computational fluid dynamics code in conjunction with the sequential linear programming method and weighting method to obtain the optimization of the plate heat exchanger with staggered pin arrays for a fixed volume. In this work [13], the flow and thermal fields are assumed to be periodic fully developed flow and heat transfer with

constant wall temperature. Recently, natural convection heat transfer in annular fin-arrays mounted on a horizontal cylinder was experimentally investigated by Yildiz and Yüncü [6]. However, Yildiz and Yüncü [6] only showed the variation of the convection heat transfer rate with the fin spacing and the difference between the base temperature and the ambient temperature. The predicted results of the Nusselt numbers given by them compared with those obtained from Churchill and Chu's correlation [14] and Morgan's correlation [15] for natural convection from a horizontal circular cylinder. Chen et al. [3] applied the finite difference method in conjunction with the least-squares scheme and experimental temperature data to predict the fin efficiency and average heat transfer coefficient on the fin inside one-tube plate finned-tube heat exchangers for a single fin and various air speeds. Later, Chen and Chou [4] also applied the same scheme to predict the fin efficiency and heat transfer coefficient on the fin inside one-tube plate finned-tube heat exchangers in natural convection for various fin spacings. Due to the consideration of the radiation and convection heat transfer coefficients, the predicted results of the average heat transfer coefficient on the fin obtained from this scheme [4] are higher than those obtained from the correlation recommended by current textbooks [1,16]. Thus, in order to validate the accuracy of this scheme further, the present study applies the similar method proposed by Chen and Chou [4] to estimate the fin efficiency and average heat transfer coefficient on the fin of annular-finned tube heat exchangers in natural convection. The present estimated results of the average natural-convection heat transfer coefficient on the annular circular fin also compare with those obtained from the correlation recommended by current textbooks [1,16].

The inverse analysis of the present study is that the whole fin is divided into several analysis sub-fin regions and then the fin temperatures at these selected measurement locations are measured using T-type thermocouples. Later, the finite difference method in conjunction with these measured temperatures and least-squares method is applied to predict the average heat transfer coefficients on these sub-fin regions. Furthermore, the average heat transfer coefficient on the whole annular circular fin $\bar{h}$ and fin efficiency can be obtained for various fin spacings under the given conditions of the ambient temperature and tube temperature.

The advantage of the present study is that the governing differential equations for the airflow do not need to be solved. In this study, the effect of the fin spacing on the estimation of the $\bar{h}$ value and fin efficiency is investigated. The computational procedures for the estimates of the average heat transfer coefficients on each sub-fin region are performed repeatedly until the sum of the squares of the deviations between the calculated and measured temperatures becomes minimum.

2. Mathematical formulation

The experimental apparatus configuration of the present study is shown in Fig. 1. The schematic diagram of one-tube annular-finned tube heat exchanger in natural convection is shown in Fig. 2. Fig. 3 shows the physical model of the two-dimensional thin annular circular fin inside one-tube annular-finned tube heat exchanger. R_o and R_i denote the outer and inner radii of the annular circular fin, respectively. S and δ respectively denote the fin spacing and fin thickness. The center of the circular tube is located at ($r = 0$, $\theta = 0$). T_o and T_∞ respectively denote the outer surface temperature of the circular tube and the ambient temperature. Due to the thin fin behavior, the temperature gradient in the z-direction (the fin thickness) is small and the fin temperature varies only in the r- and θ-directions. The "insulated tip" assumption can be an adequate approximation provided that the actual heat rate dissipated through the tip is much smaller than the total heat rate drawn from the base wall [17]. It can be found from the works of Chen et al. [3], Chen and Chou [4], Saboya and Sparrow [10], Rosman et al. [11] and Ay et al. [12] that the heat transfer coefficient on the fin inside the plate

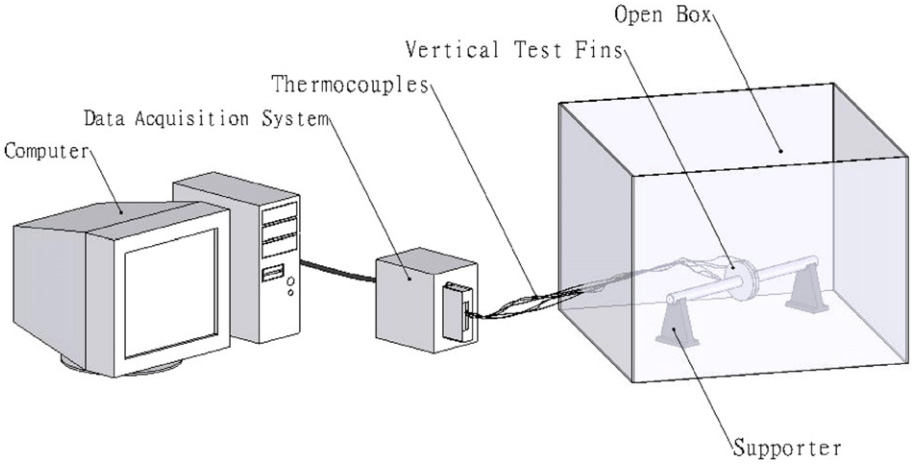

Fig. 1. Experimental apparatus configuration of the present study.

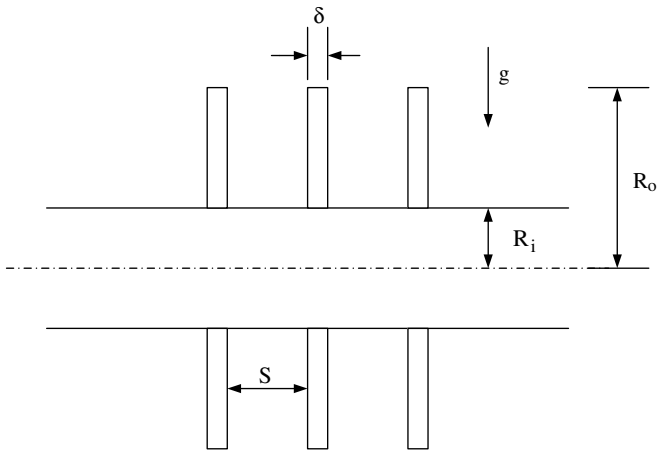

Fig. 2. Schematic diagram of one-tube plate fin heat exchangers with the fin spacing.

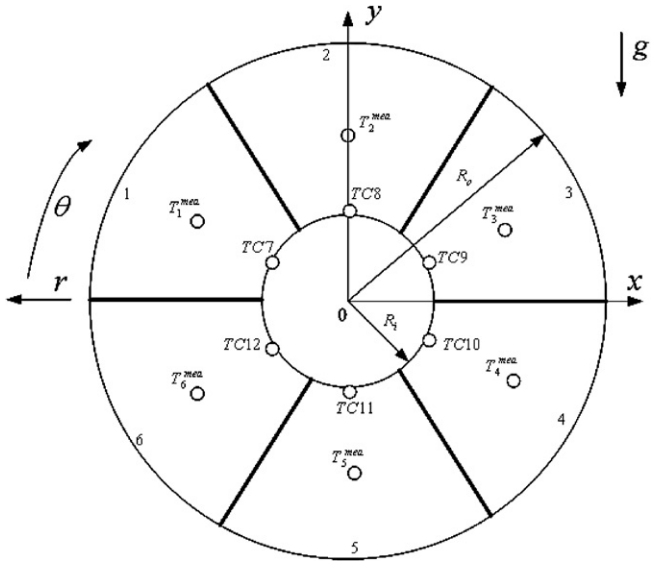

Fig. 3. Physical geometry of a two-dimensional annular circular fin with measurement locations and sub-fin regions.

finned-tube heat exchangers is very non-uniform. Thus the heat transfer coefficient $h(r,\theta)$ in the present study is also assumed to be non-uniform. The local heat transfer coefficient on the fin inside an annular-finned tube heat exchanger can be estimated provided that the fin temperatures at various measurement locations can be measured. Under the assumptions of the steady state and constant thermal properties, the two-dimensional heat conduction equation for the continuous thin fin of one-tube annular-finned tube heat exchangers can be expressed as

$$\frac{\partial^2 T}{\partial r^2}+\frac{1}{r}\frac{\partial T}{\partial r}+\frac{1}{r^2}\frac{\partial^2 T}{\partial \theta^2}=\frac{2h(r,\theta)}{k\delta}(T-T_\infty)\quad \text{in } R_i<r<R_o,\ 0<\theta\leqslant 2\pi \tag{1}$$

Its corresponding boundary conditions are

$$\frac{\partial T(r,0)}{\partial \theta}=\frac{\partial T(r,2\pi)}{\partial \theta} \tag{2}$$

$$T(r,0)=T(r,2\pi) \tag{3}$$

$$T(r,\theta)=T_o \quad \text{at } r=R_i \tag{4}$$

and

$$\frac{\partial T(r,\theta)}{\partial r}=0 \quad \text{at } r=R_o \tag{5}$$

where T is the fin temperature. r and θ are cylindrical coordinates. $h(r,\theta)$ is the heat transfer coefficient. k is the thermal conductivity of the fin.

3. Numerical analysis

It might be difficult to measure the temperature distributions on the whole annular circular fin using the infrared thermography and thermocouples for some practical heat transfer problems. Relatively, the unknown heat transfer coefficient $h(r,\theta)$ on a fin is not easy to be obtained. Under this circumstance, the whole annular circular fin considered can be divided into N sub-fin regions in the present inverse scheme and then the unknown heat transfer coefficient on each sub-fin region can be assumed to be constant. Thus the application of the finite difference method to Eq. (1) can produce the following difference equation on the kth sub-fin region:

$$\begin{aligned}&\frac{T_{i,j+1}-2T_{i,j}+T_{i,j-1}}{\ell_r^2}+\frac{1}{R_i+(j-1)\ell_r}\frac{T_{i,j+1}-T_{i,j-1}}{2\ell_r}\\&+\frac{1}{[R_i+(j-1)\ell_r]^2}\frac{T_{i+1,j}-2T_{i,j}+T_{i-1,j}}{\ell_\theta^2}\\&=\frac{2\bar{h}_k}{k\delta}(T_{i,j}-T_\infty)\\&\text{for } i=\frac{(N_\theta-1)(k-1)}{N}+2,\frac{(N_\theta-1)(k-1)}{N}+3,\ldots,\frac{(N_\theta-1)}{N}k,\\&j=2,\ldots,N_r\end{aligned} \tag{6}$$

where ℓ_r and ℓ_θ respectively are the distance between two neighboring nodes in the r- and θ-directions and are defined as $\ell_r=(R_0-R_i)/(N_r-1)$ and $\ell_\theta=2\pi/(N_\theta-1)$. N_r and N_θ are the nodal numbers in the r- and θ-directions, respectively. $\bar{h}_k$ denotes the average heat transfer coefficient on the kth sub-fin region.

The application of the central difference approximation to the boundary condition (2) and then substitution of the resulting equation into Eq. (6) can yield the difference equations as

$$\begin{aligned}&\frac{T_{1,j+1}-2T_{1,j}+T_{1,j-1}}{\ell_r^2}+\frac{1}{R_i+(j-1)\ell_r}\frac{T_{1,j+1}-T_{1,j-1}}{2\ell_r}\\&+\frac{1}{[R_i+(j-1)\ell_r]^2}\frac{T_{2,j}-2T_{1,j}+T_{N_\theta-1,j}}{\ell_\theta^2}\\&=\frac{2\bar{h}_m}{k\delta}(T_{1,j}-T_\infty)\quad \text{for } j=2,3,\ldots,N_r\end{aligned} \tag{7}$$

and

$$\frac{T_{N_\theta,j+1}-2T_{N_\theta,j}+T_{N_\theta,j-1}}{\ell_r^2}+\frac{1}{R_i+(j-1)\ell_r}\frac{T_{N_\theta,j+1}-T_{N_\theta,j-1}}{2\ell_r}+\frac{1}{[R_i+(j-1)\ell_r]^2}\frac{T_{2,j}-2T_{N_\theta,j}+T_{N_\theta-1,j}}{\ell_\theta^2}=\frac{2\bar{h}_m}{k\delta}(T_{N_\theta,j}-T_\infty)\quad \text{for } j=2,3,\ldots,N_r \tag{8}$$

where $\bar{h}_m$ is defined as $\bar{h}_m=(\bar{h}_1+\bar{h}_N)/2$.

The discretized form of Eq. (4) is given as

$$T_{i,1}=T_o\quad \text{for } i=1,2,\ldots,N_\theta \tag{9}$$

The application of the central difference approximation to the boundary conditions (3) and (5) can yield their difference equations as

$$T_{1,j}=T_{N_\theta,j}\quad \text{for } j=2,\ldots,N_r \tag{10}$$

and

$$T_{i,N_r-1}=T_{i,N_r+1}\quad \text{for } i=1,2,\ldots,N_\theta \tag{11}$$

The difference equations for the nodes at the interface of two neighboring sub-fin regions, as shown in Fig. 4, can be expressed as

$$\frac{T_{i,j+1}-2T_{i,j}+T_{i,j-1}}{\ell_r^2}+\frac{1}{R_i+(j-1)\ell_r}\frac{T_{i,j+1}-T_{i,j-1}}{2\ell_r}+\frac{1}{[R_i+(j-1)\ell_r]^2}\frac{T_{i+1,j}-2T_{i,j}+T_{i-1,j}}{\ell_\theta^2}=\frac{(\bar{h}_k+\bar{h}_{k+1})}{k_f\delta}(T_{i,j}-T_\infty) \tag{12}$$

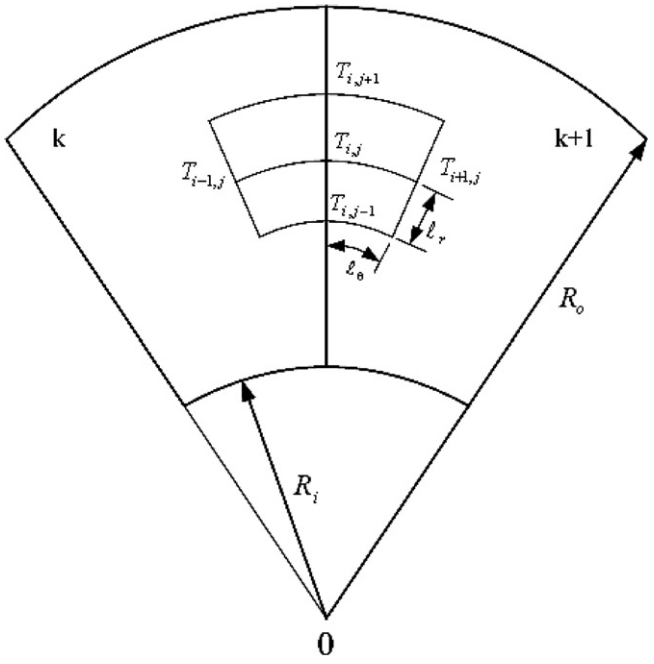

Fig. 4. Nodes at the interface of two-neighboring sub-fin areas.

Rearrangement of Eqs. (6)–(12) can yield the following matrix equation:

$$[A][T]=[F] \tag{13}$$

where $[A]$ is a global conduction matrix. $[T]$ is a matrix representing the nodal temperatures. $[F]$ is a force matrix. The nodal temperatures can be obtained from Eq. (13) using the Gauss elimination algorithm.

Once the heat transfer coefficient on each sub-fin region is obtained, the heat rate dissipated from the jth sub-fin region q_j and average heat transfer coefficient on the whole annular circular fin $\bar{h}$ can be determined. The heat rate dissipated from the jth sub-fin region q_i is defined as

$$q_i=2\bar{h}_j\int_{A_j}(T-T_\infty)\mathrm{d}A\quad \text{for } j=1,2,\ldots,N \tag{14}$$

The average heat transfer coefficient on the whole fin $\bar{h}$ can be expressed as

$$\bar{h}=\sum_{j=1}^{N}\bar{h}_jA_j/A_f \tag{15}$$

where A_f is the area of the annular circular fin.

The efficiency of the annular circular fin η_f is defined as the ratio of the actual heat rate from the annular circular fin to the dissipated heat rate from the fin maintained at the tube temperature T_o. Thus the fin efficiency η_f can be expressed as

$$\eta_f=\frac{\sum_{j=1}^{N}q_j}{2A_f(T_o-T_\infty)\bar{h}} \tag{16}$$

The total heat rate dissipated from the whole fin to the ambient Q can be written as

$$Q=\sum_{j=1}^{N}q_j \tag{17}$$

In order to estimate the unknown heat transfer coefficient on the jth sub-fin region $\bar{h}_j$, the additional information of the steady-state measured temperatures is required at N interior measurement locations. The more a number of the sub-fin regions are, the more accurate the estimation of the unknown average heat transfer coefficient on the whole annular circular fin can be. Relatively, a more computational time and the number of the thermocouple can be increased. Moreover, the increase of the thermocouple can affect the flow and thermal fields. In order to validate the accuracy of the present inverse scheme, an example with the heat transfer coefficient $h(r,\theta)=5-2r\sin\theta$ is illustrated. It can be found from Table 1 that the present estimates of $\bar{h}$ using six and eight sub-regions both are in good agreement with the exact solution for the limit of error of the thermocouple $\omega_j=0$. In the present study, T-type thermocouples are used to record the temperature information at selected measurement locations. The measured temperature taken from the jth thermocouple is denoted by T_j^{mea}, $j=1,\ldots,N$, as shown in Table 2.

Table 1
Comparison of the h_j and $\bar{h}$ values for $h(r,\theta) = 5 - 2r\sin\theta$, $T_o = 360$ K, $T_\infty = 298$ K, $w_j = 0$ and various sub-regions

	T_j^{mea} (K)	$\bar{h}_j$ (W/m^2 K)		$\bar{h}$ (W/m^2 K)	
		Present estimates	Exact	Present estimates	Exact
Six sub-regions	$T_1^{mea} = 337.28$	$\bar{h}_1 = 4.96$	$\bar{h}_1 = 4.97$	5.00	5.00
	$T_2^{mea} = 337.36$	$\bar{h}_2 = 4.92$	$\bar{h}_2 = 4.94$		
	$T_3^{mea} = 337.28$	$\bar{h}_3 = 4.96$	$\bar{h}_3 = 4.97$		
	$T_4^{mea} = 337.14$	$\bar{h}_4 = 5.04$	$\bar{h}_4 = 5.03$		
	$T_5^{mea} = 337.07$	$\bar{h}_5 = 5.08$	$\bar{h}_5 = 5.07$		
	$T_6^{mea} = 337.14$	$\bar{h}_6 = 5.04$	$\bar{h}_6 = 5.03$		
Eight sub-regions	$T_1^{mea} = 337.27$	$\bar{h}_1 = 4.97$	$\bar{h}_1 = 4.98$	5.00	5.00
	$T_2^{mea} = 337.35$	$\bar{h}_2 = 4.93$	$\bar{h}_2 = 4.94$		
	$T_3^{mea} = 337.35$	$\bar{h}_3 = 4.93$	$\bar{h}_3 = 4.94$		
	$T_4^{mea} = 337.27$	$\bar{h}_4 = 4.97$	$\bar{h}_4 = 4.98$		
	$T_5^{mea} = 337.15$	$\bar{h}_5 = 5.04$	$\bar{h}_5 = 5.02$		
	$T_6^{mea} = 337.08$	$\bar{h}_6 = 5.06$	$\bar{h}_6 = 5.06$		
	$T_7^{mea} = 337.08$	$\bar{h}_7 = 5.06$	$\bar{h}_7 = 5.06$		
	$T_8^{mea} = 337.15$	$\bar{h}_8 = 5.04$	$\bar{h}_8 = 5.02$		

The least-squares minimization technique is applied to minimize the sum of the squares of the deviations between the calculated and measured temperatures at selected measurement locations. In the present study, the unknown average heat transfer coefficients on each sub-fin region $\bar{h}_k$ can be expressed as

$$\bar{h}_k = C_k \quad \text{for } k = 1, 2, \ldots, N \tag{18}$$

The error in the estimates $E(C_1, C_2, \ldots, C_N)$ is minimized and is defined as

$$E(C_1, C_2, \ldots, C_N) = \sum_{j=1}^{N} [T_j^{cal} - T_j^{mea}]^2 \tag{19}$$

where the calculated temperature taken from the jth thermocouple location, T_j^{cal}, is taken from Eq. (13).

The estimated values of C_i, $i = 1, 2, \ldots, N$, are determined until the value of $E(C_1, C_2, \ldots, C_N)$ is minimum. The computational procedures for estimating the C_i value, $i = 1, 2, \ldots, N$, are described as follows.

First, the initial guesses of C_i, $i = 1,2, \ldots, N$, are arbitrarily chosen. Later, the calculated temperature T_j^{cal} can be determined. Deviation of T_j^{mea} and T_j^{cal}, e_j, is expressed as

$$e_j = T_j^{cal} - T_j^{mea} \quad \text{for } j = 1, 2, \ldots, N \tag{20}$$

The new calculated temperature $T_j^{cal,n}$ can be expanded in a first-order Taylor series approximation as

$$T_j^{cal,n} = T_j^{cal} + \sum_{k=1}^{N} \frac{\partial T_j^{cal}}{\partial C_k} \mathrm{d}C_k \quad \text{for } j = 1, 2, \ldots, N \tag{21}$$

In order to obtain the $\frac{\partial T_j^{cal}}{\partial C_k}$ value, the new estimated value C_k^* is introduced and is expressed as

$$C_k^* = C_k + d_k \delta_{jk} \quad \text{for } j, k = 1, 2, \ldots, N \tag{22}$$

where d_k denotes the correction. The symbol δ_{jk} is Kronecker delta.

Accordingly, the new calculated temperature $T_j^{cal,n}$ with respect to C_k^* can be determined from Eq. (13). Deviation of $T_j^{cal,n}$ and T_j^{mea}, e_j^n, can be defined as

$$e_j^n = T_j^{cal,n} - T_j^{mea} \quad \text{for } j = 1, 2, \ldots, N \tag{23}$$

The finite difference representation of the derivative $\frac{\partial T_j^{cal}}{\partial C_k}$ can be expressed as

$$w_j^k = \frac{\partial T_j^{cal}}{\partial C_k} = \frac{T_j^{cal,n} - T_j^{cal}}{C_k^* - C_k} \quad \text{for } j, k = 1, 2, \ldots, N \tag{24}$$

Substitution of Eqs. (20), (22), (23) into Eq. (24) can yield

$$w_j^k = \frac{e_j^n - e_j}{d_k} \quad \text{for } j, k = 1, 2, \ldots, N \tag{25}$$

Substitution of Eq. (24) into Eq. (21) can obtain the new expression of $T_j^{cal,n}$ as

$$T_j^{cal,n} = T_j^{cal} + \sum_{k=1}^{N} w_j^k d_k^* \quad \text{for } j = 1, 2, \ldots, N \tag{26}$$

where $d_k^* = \mathrm{d}C_k$ denotes the new correction of the C_k value.

Substituting Eqs. (20) and (23) into Eq. (26) gives

$$e_j^n = e_j + \sum_{k=1}^{N} w_j^k d_k^* \quad \text{for } j = 1, 2, \ldots, N \tag{27}$$

As shown in Eq. (19), the error in the estimates $E(C_1 + \Delta C_1, C_2 + \Delta C_2, \ldots, C_N + \Delta C_N)$ can be expressed as

$$E(C_1 + \Delta C_1, C_2 + \Delta C_2, \ldots, C_N + \Delta C_N) = \sum_{j=1}^{N} (e_j^n)^2 \tag{28}$$

In order to yield the minimum value of E with respect to the C_k values, $k = 1, 2, \ldots, N$, differentiating E with respect to the new correction d_k^* will be performed. Thus the correction equations for the C_k values can be expressed as

$$\sum_{i=1}^{N} \sum_{k=1}^{N} w_k^j w_k^i d_i^* = -\sum_{i=1}^{N} w_i^j e_i \quad j = 1, 2, \ldots, N \tag{29}$$

Table 2
Temperature measurements and the present estimates for various T_o, T_∞ and S values

	$S = 0.005$ m, $T_o = 357.72$ K, $T_\infty = 300.93$ K	$S = 0.01$ m, $T_o = 351.24$ K, $T_\infty = 298.45$ K	$S = 0.02$ m, $T_o = 351.95$ K, $T_\infty = 300.97$ K	$S \to \infty$, $T_o = 353.42$ K, $T_\infty = 300.86$ K
T_j^{mea} (K)	$T_1^{mea} = 336.84$	$T_1^{mea} = 324.61$	$T_1^{mea} = 324.50$	$T_1^{mea} = 323.33$
	$T_2^{mea} = 341.63$	$T_2^{mea} = 332.50$	$T_2^{mea} = 329.09$	$T_2^{mea} = 329.27$
	$T_3^{mea} = 335.19$	$T_3^{mea} = 321.96$	$T_3^{mea} = 324.09$	$T_3^{mea} = 324.66$
	$T_4^{mea} = 327.40$	$T_4^{mea} = 317.63$	$T_4^{mea} = 319.45$	$T_4^{mea} = 320.14$
	$T_5^{mea} = 325.78$	$T_5^{mea} = 316.99$	$T_5^{mea} = 315.77$	$T_5^{mea} = 316.39$
	$T_6^{mea} = 328.18$	$T_6^{mea} = 318.31$	$T_6^{mea} = 318.41$	$T_6^{mea} = 318.72$
$\bar{h}_j$ (W/m^2 K)	$\bar{h}_1 = 4.256$	$\bar{h}_1 = 9.772$	$\bar{h}_1 = 9.796$	$\bar{h}_1 = 12.372$
	$\bar{h}_2 = 1.411$	$\bar{h}_2 = 0.007$	$\bar{h}_2 = 4.303$	$\bar{h}_2 = 4.243$
	$\bar{h}_3 = 5.439$	$\bar{h}_3 = 13.335$	$\bar{h}_3 = 10.886$	$\bar{h}_3 = 10.898$
	$\bar{h}_4 = 11.537$	$\bar{h}_4 = 16.182$	$\bar{h}_4 = 15.147$	$\bar{h}_4 = 14.799$
	$\bar{h}_5 = 11.890$	$\bar{h}_5 = 16.471$	$\bar{h}_5 = 24.177$	$\bar{h}_5 = 23.495$
	$\bar{h}_6 = 11.052$	$\bar{h}_6 = 15.977$	$\bar{h}_6 = 17.773$	$\bar{h}_6 = 17.309$
q_j (W)	$q_1 = 0.402$	$q_1 = 0.731$	$q_1 = 0.669$	$q_1 = 0.834$
	$q_2 = 0.145$	$q_2 = 0.001$	$q_2 = 0.\ 326$	$q_2 = 0.326$
	$q_3 = 0.498$	$q_3 = 0.\ 938$	$q_3 = 0.738$	$q_3 = 0.761$
	$q_4 = 0.894$	$q_4 = 0.\ 991$	$q_4 = 0.889$	$q_4 = 0.901$
	$q_5 = 0.879$	$q_5 = 0.\ 982$	$q_5 = 1.268$	$q_5 = 1.282$
	$q_6 = 0.850$	$q_6 = 0.\ 965$	$q_6 = 0.972$	$q_6 = 0.968$
$\bar{h}$ (W/m^2 K)	7.598	11.957	13.680	13.852
Q (W)	3.668	4.610	4.862	5.072
η_f	0.597	0.513	0.489	0.488

Eq. (29) is a set of N algebraic equations for the new correction d_k^*. The new correction d_k^* can be obtained by solving Eq. (29). Furthermore, the new estimated heat transfer coefficients can also be determined. The above procedures are repeated until the values of $\left|\frac{T_j^{mea} - T_j^{cal}}{T_j^{mea}}\right|$, $j = 1, 2, \ldots, N$, are all less than 10^{-6}. An iteration process takes about 30 s for each case.

4. Experimental apparatus

The schematic diagram of the experimental apparatus used in the present study for the estimation of the natural-convection heat transfer coefficient on an annular circular fin of one-tube finned-tube heat exchangers is shown in Fig. 1. This experiment is conducted in an open box, as shown in Fig. 1. This box with 550 mm in length, 450 mm in width and 300 mm in height is made of acrylic-plastic sheets. The horizontal circular tube with an outer diameter of 27 mm and 2 mm in thickness and the test annular circular fin with 27 mm in inner diameter, 99 mm in outer diameter and 1 mm in thickness are made of AISI 304 stainless material. It can be found from Ref. [18] that the thermal conductivity of AISI 304 stainless material is 14.9 W/m K. The horizontal circular tube is placed on two steel supporters, which is 100 mm above an experimental table to prevent ground effects. The test fins are vertically mounted on this circular tube, as shown in Figs. 1 and 2. The ambient temperature and test fin temperature are measured using T-type thermocouples. A cylindrical rod with an outer diameter of 20 mm and 300 mm in length bound by a single thermofoil heater with an outer diameter of 1.5 mm is inserted in the circular tube and then the tube will be heated. Thus the radial gap between the surrounding circular tube and the whole electrical heating rod is small. On the other hand, the whole electrical heating rod is nearly fitted to the surrounding circular tube. Power input (200 W) is supplied to the heater. The steady-state condition in the present study has reached about 2000 s. The readings of all the thermocouples used to measure the ambient temperature, tube temperature and fin temperature are recorded from $t = 0$ until the steady-state condition has reached. All the data signals were collected and converted by a data acquisition system (National Instruments NI SCXI-1000, 1102, 1300). The data acquisition system then transmitted the converted signals through a Data Acquisition Board to a personal computer in conjunction with a Labview software for further operation. The limit of error of the T-type thermocouple for $0° \leqslant T \leqslant 350$ °C is $\pm 0.4\%$. The histories of the measured temperatures for all the thermocouples are obtained using the least-squares fitting method. The experiment will be repeatedly made provided that one of the temperature measurements obtained from all the thermocouples is not very accurate. In order to check the accuracy of the measured temperatures, the experiments are at least repeated two times. The ambient temperature T_∞ is installed at 100 mm away from the test specimen. In order to minimize the effect of the thermal contact resistance between the fin and the circular tube on the estimates, the gap between the fin and the circular tube is filled with the cyanoacrylate adhesive (Satlon, D-3). In addition, six thermocouples placed in the interface between the fin and the circular tube are fixed at six different positions of the fin base, TC7, TC8,

TC9, TC10, TC11 and TC12 shown in Fig. 3, by using a cyanoacrylate adhesive. These six thermocouples are adhered at $\pi/6$, $\pi/2$, $5\pi/6$, $7\pi/6$, $3\pi/2$ and $11\pi/6$ in angle. The fin base temperatures are measured from these six thermocouples. These six temperature measurements do not deviate much from each other. Thus the average of these six temperature measurements is taken as the fin base temperature and the outer surface temperature of the circular tube T_0 in the present study. It is known that there exists a complex flow pattern within an annular-finned tube heat exchanger in natural convection due to a plume of the heated air rising above the horizontal heated circular tube at a uniform temperature T_0, which is higher than the ambient temperature T_∞. The thermal boundary layer starts to develop at the bottom of the heated tube and increases in thickness along the circumference of this tube. Thus this airflow forms a low-velocity region above the heated tube. This implies that the fin base temperature at the position of TC8 is the highest temperature, and the fin temperature on the top fin region of the tube or Region 2 is also markedly higher than those on other fin regions for various T_0, T_∞ and S values, as shown in Table 2. The similar result can also be observed from Ref. [4]. For the present problem, the flow and thermal fields in the previous works were often assumed to be symmetric. In order to investigate the reliability of the above assumption further, the regular arrangements of the thermocouples adhered on the fin are chosen. Thus the whole annular circular fin is divided into six regions, i.e., $N = 6$. Regions 1–3 are on the regions above the x-axis. Regions 4–6 are on the regions below the x-axis. In order to estimate the average heat transfer coefficient on each sub-fin region, six T-type thermocouples are adhered at the suitable positions of the sub-fin region, as shown in Fig. 3. Six T-type thermocouples for the measurements of the fin temperature are adhered at 33.5 mm in radius from the center of the circular tube and at $\pi/6$, $\pi/2$, $5\pi/6$, $7\pi/6$, $3\pi/2$ and $11\pi/6$ in angle. It is observed that six thermocouples are installed at symmetric positions with respect to the center of the annular circular fin, and the first, third, fourth and sixth thermocouples are symmetric with respect to the y-axis. The diameter of the spot size attached to the fin using the cyanoacrylate adhesive for all the thermocouples is about 0.3 mm.

5. Results and discussion

It can be observed from Ref. [17] that the "insulated tip" assumption is a good approximation when the actual heat rate passed through the tip is negligible relative to the total heat rate drawn from the base wall. For simplicity, the average heat transfer coefficient on the tip surface can be assumed to be the same as that on the lateral surface of the fin. On the other hand, the "insulated tip" assumption will be reasonable provided that the surface area of the fin tip is very smaller than the total fin surface area. Their ratio for the present study can be written as $\frac{R_o\delta}{(R_o^2-R_i^2)+R_o\delta}$. Based on experiment data given in the present study, the surface area of the fin tip is only 2.14% of the total fin surface area. This implies that the heat rate passed through the fin tip can be neglected in the present study. Thus Eq. (5) in the present study should be the reasonable assumption. The values of $T_1^{\mathrm{mea}}(33.5, \pi/6)$, $T_2^{\mathrm{mea}}(33.5, \pi/2)$, $T_3^{\mathrm{mea}}(33.5, 5\pi/6)$, $T_4^{\mathrm{mea}}(33.5, 7\pi/6)$, $T_5^{\mathrm{mea}}(33.5, 3\pi/2)$ and $T_6^{\mathrm{mea}}(33.5, 11\pi/6)$ respectively denote T_1^{mea}, T_2^{mea}, T_3^{mea}, T_4^{mea}, T_5^{mea} and T_6^{mea}. The measured temperatures T_1^{mea}, T_2^{mea}, T_3^{mea}, T_4^{mea}, T_5^{mea} and T_6^{mea} for various T_0, T_∞ and S values are shown in Table 2. The nodal numbers N_r and N_θ used in all the computations are $N_r = 10$ and $N_\theta = 49$. Table 2 also shows the effect of the fin spacing S on the average heat transfer coefficient on the jth sub-fin region $\bar{h}_j$, heat rate on the jth sub-fin region q_j, total heat rate on the whole annular circular fin Q, average heat transfer coefficient on the whole annular circular fin $\bar{h}$ and fin efficiency η_f. The measured temperatures shown in Table 2 display $T_1^{\mathrm{mea}} \neq T_3^{\mathrm{mea}}$ and $T_4^{\mathrm{mea}} \neq T_6^{\mathrm{mea}}$. This phenomenon can result from the measurement error and the following reasons that the flow pattern of the present problem around the tube may become random in motion and the test annular-finned tube heat exchanger can not be easy to be horizontally positioned. Thus the symmetric assumptions of the flow and thermal fields are not always very reasonable for the present problem. It can be found from Table 2 that the heat transfer coefficient on the top fin region of the horizontal circular tube or Region 2 is lower than those on other sub-fin regions for various S values because this region belongs to a low-performance region. On the other hand, the heat transfer coefficient is highest on the bottom region of the tube and is lowest on the top region of the tube. The same results can be found from Ref. [4]. Thus the present estimated results further show that the assumption of the constant heat transfer coefficient on the whole annular circular fin is not always reasonable for the present problem. This implies that the actual steady-state heat transfer coefficient on the fin of annular-finned tube heat exchanger should be the function of position. The ratio of the average heat transfer coefficient on the bottom fin region of the tube $\bar{h}_5$ to that on the top fin region of the tube $\bar{h}_2$ can be up to about 8.43 times for $S = 0.005$ m and is about 5.62 times for $S = 0.02$ m. The $\bar{h}$ value for $S = 0.02$ m is approximately 80% higher than that for $S = 0.005$ m. However, the Q value for $S = 0.02$ m can be up to 32.6% higher than that for $S = 0.005$ m. Thus the effect of the fin spacing on $\bar{h}$ and Q is not negligible. It can be found from Table 2 that the heat rate on Region 2 in the range of $S \geqq 0.005$ m is responsible for 0.1–6.7% of the total heat rate on the whole annular circular fin. Therefore, in order to enhance the overall heat transfer, it is desirable to find a way to increase heat transfer in Region 2. This may lead to design a heat exchanger with a high heat transfer performance. Table 2 also shows that the fin efficiency η_f decreases with increasing the S value and decreases from 59.7% to 48.8% in the range of $S \geqq 0.005$ m. This implies that the η_f value on the annular circular fin of one-circular tube plate

finned-tube heat exchangers is higher than that on a vertical square fin [4] under the same conditions.

Variations of the average heat transfer coefficient $\bar{h}$ and fin efficiency η_f with the fin spacing S are shown in Figs. 5 and 6. It is known that a resistance to the natural convective airflow in the fin arrays increases with decreasing the fin spacing S for the present problem. On the other hand, this resistance has a negligible effect on the average heat transfer coefficient and fin efficiency as $S \to \infty$. It can be found from Figs. 5 and 6 that the average heat transfer coefficient $\bar{h}$ increases with increasing the S value. However, the fin efficiency η_f decreases with increasing the S value. The average heat transfer coefficient $\bar{h}$ and fin efficiency η_f can approach their corresponding asymptotical value obtained from a single annular circular fin when the fin spacing exceeds a certain value, as shown in Figs. 5 and 6. The tendency of these predicted results shown in Figs. 5 and 6 is the same as that shown in Ref. [4]. These findings further lead to support the methodology of the present experiments and inverse analysis. The effect of the fin spacing S on the $\bar{h}$ and η_f values shown in Figs. 5 and 6 can be negligible when the S value exceeds about 0.015 m. Fig. 7 shows the effect of the Rayleigh number Ra_s on the fin efficiency η_f. The smoothing curves can be applied to match the data points of $\eta_f - Ra_s^{1/4}$. The correlation of $\eta_f - Ra_s^{1/4}$ can be obtained using the least-square fitting method of experimental data and are expressed as

$$\eta_f = 0.8397 - 0.1777 \times Ra_s^{1/4} + 0.0306(Ra_s^{1/4})^2 - 0.0018(Ra_s^{1/4})^3 \quad (30)$$

where the Rayleigh number Ra_s is defined as

$$Ra_s = \frac{g\beta(T_0 - T_\infty)S^3}{v\alpha}\left(\frac{S}{D}\right) \quad (31)$$

In Eq. (31), the properties β, α and v respectively denote the volumetric thermal expansion coefficient, thermal diffusivity and kinematic viscosity of the air. Thus the Ra_s value ranges about from 15 to ∞ in the present study.

It can be found from the books of Raithby and Hollands [1] and Kreith and Bohn [16] that the empirical relation of Nu_s and Ra_s for long isothermal annular circular fins can be expressed as

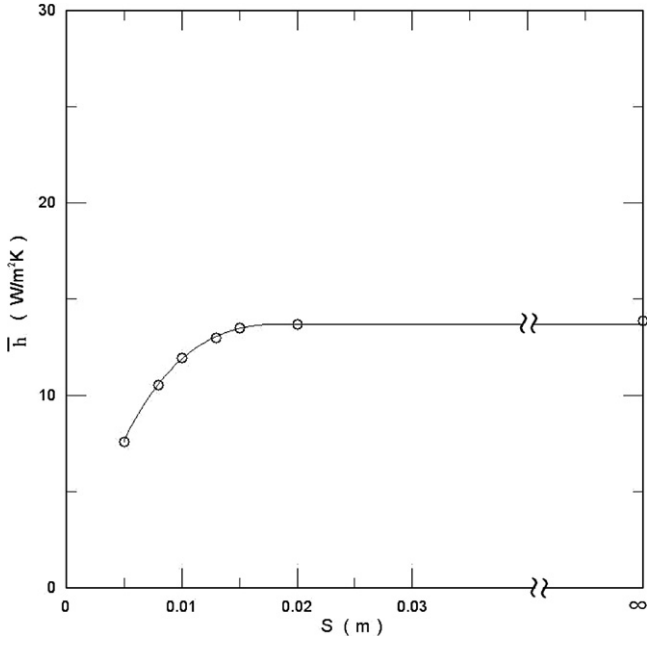

Fig. 5. Variation of $\bar{h}$ with S.

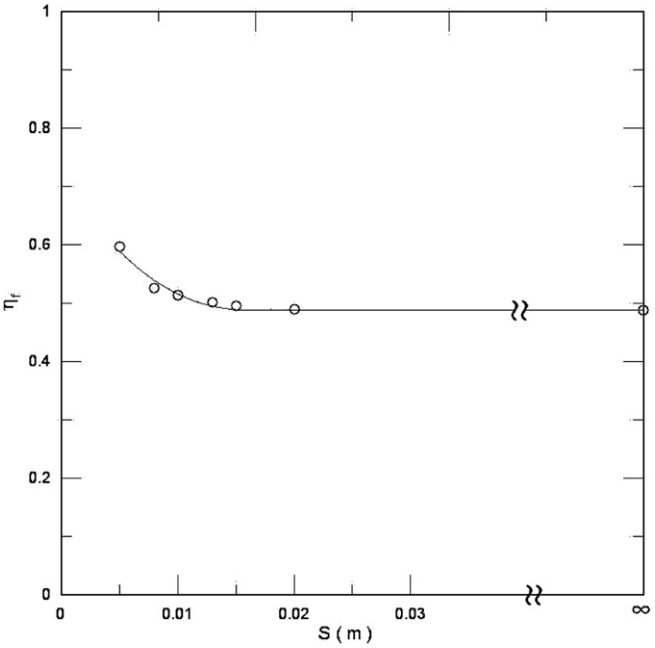

Fig. 6. Variation of η_f with S.

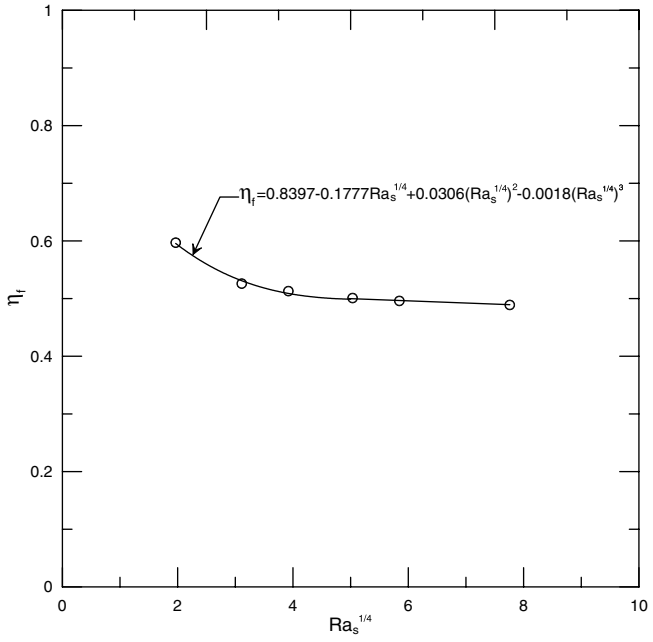

Fig. 7. Variation of η_f with $Ra_s^{1/4}$.

$$Nu_s = \frac{Ra_s}{12\pi}\left\{2 - \exp\left[-\left(\frac{C^*}{Ra_s}\right)^{3/4}\right] - \exp\left[-\beta^*\left(\frac{C^*}{Ra_s}\right)^{3/4}\right]\right\} \quad \text{for } 1.67 < \xi < \infty \tag{32}$$

where the parameter ξ denotes the ratio of the outer radius of the annular fin to the inner radius of the annular fin and is defined as $\xi = R_o/R_i$. All the properties are evaluated at the wall temperature T_o. Nu_s, β^* and C^* are defined as

$$Nu_s = \frac{\bar{h}S}{k_{air}} \tag{33}$$

$$\beta^* = (0.17/\xi) + e^{-(4.8/\xi)} \tag{34}$$

and

$$C^* = \left\{\frac{23.7 - 1.1[1 + (152/\xi^2)]^{1/2}}{1 + \beta^*}\right\}^{4/3} \tag{35}$$

In Eq. (33), k_{air} denotes the thermal conductivity of the air.

It is known that heat is transferred to the surroundings by natural convection and radiation for the present problem. On the other hand, the radiation heat transfer may be quite significant in natural convection [19]. However, the natural-convection heat loss can decrease more rapidly than the radiation heat loss with decreasing the fin spacing. Table 3 shows the comparison of the $\bar{h}$ value between the present estimates and those obtained from Eq. (32) for various S and Ra_s values. It can be observed from Table 3 that the present estimates of the $\bar{h}$ value range from 7.598 $W/m^2 K$ to 13.680 $W/m^2 K$ for $0.02\ m \geqslant S \geqslant 0.005\ m$. However, the $\bar{h}$ value obtained from the correlation in the books of Raithby and Hollands [1] and Kreith and Bohn [16] ranges from 3.118 $W/m^2 K$ to 5.888 $W/m^2 K$ for $S \geqslant 0.005$ m under the condition of the ideal isothermal situation. In order to validate the reliability of the present inverse scheme, a comparison between the present estimates of the $\bar{h}$ value under the condition of the ideal isothermal situation and those obtained from the correlation in the textbooks of Raithby and Hollands [1] and Kreith and Bohn [16] is made. The present estimate of the average heat transfer coefficient on the fin under the condition of the ideal isothermal situation $\bar{h}^{iso}$ can be determined from the following expression:

$$Q = \sum_{j=1}^{N} 2\bar{h}_j \int_{A_j} (T - T_\infty)dA = 2\bar{h}^{iso}A_f(T_o - T_\infty) \tag{36}$$

Table 3
Comparison of the heat transfer coefficient for various S and Ra_s values

S (m)	Ra_s	Present estimates		$\bar{h}^{iso}$ ($W/m^2 K$) Eq. (32)
		$\bar{h}$ ($W/m^2 K$)	$\bar{h}^{iso}$ ($W/m^2 K$)	
0.005	14.924	7.598	4.532	3.118
0.008	93.659	10.528	5.543	4.883
0.01	236.169	11.957	6.128	5.437
0.013	641.864	13.022	6.526	5.645
0.015	1166.830	13.493	6.690	5.771
0.02	3625.090	13.680	6.693	5.888

It is found from Table 3 that the present estimates of the $\bar{h}^{iso}$ value are slightly higher than those obtained from Eq. (32). This phenomenon can result from the simultaneous consideration of the convection and radiation heat transfer coefficients in the present study. The results shown in Table 3 display that the asymptotical values of the $\bar{h}$ values obtained from the present inverse scheme and Eq. (32) seem to be reached to those obtained from a single fin as $S \to \infty$. It can be found from the textbook of Kreith and Bohn [16] that the natural-convection heat transfer coefficient for the ambient air ranges from 6 $W/m^2 K$ to 30 $W/m^2 K$. Obviously, the present estimates of $\bar{h}$ shown in Table 3 lie in this range for $S \geqslant 0.005$ m. Thus the present estimates are reasonable.

Fig. 8 shows the effect of the Rayleigh number Ra_s on the Nusselt number Nu_s. The smoothing curves can be applied to match the data points of $Nu_s - Ra_s^{1/4}$. The corrections of $Nu_s - Ra_s^{1/4}$ can be obtained using the least-square fitting method of experimental data and are expressed as

$$Nu_s = -1.432 + 1.412 \times Ra_s^{1/4} \quad \text{for the nonisothermal situation} \tag{37}$$

and

$$Nu_s = -0.516 + 0.667 \times Ra_s^{1/4} \quad \text{for the isothermal situation} \tag{38}$$

The correction of $Nu_s - Ra_s^{1/4}$ obtained from Eq. (32) is expressed as

$$Nu_s = -0.553 + 0.6 \times Ra_s^{1/4} \tag{39}$$

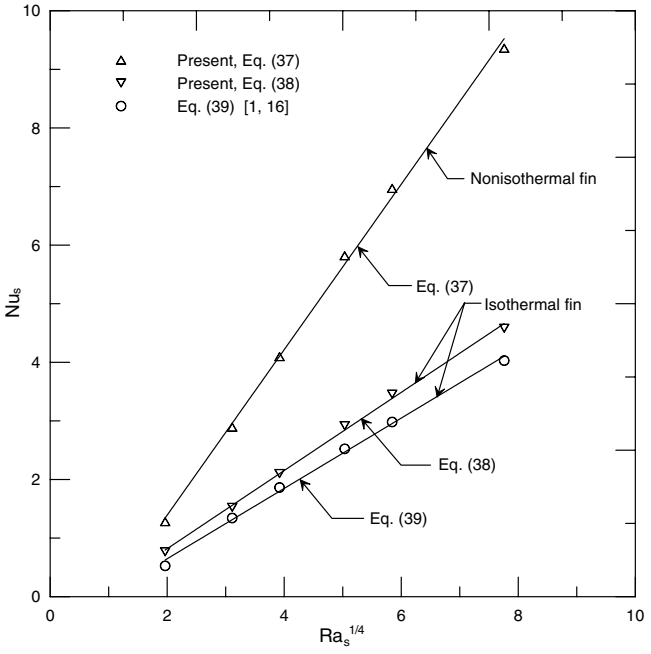

Fig. 8. Variation of Nu_s with $Ra_s^{1/4}$.

Examination of Table 3 shows that the deviation between the present estimates of the $\bar{h}^{iso}$ value and those obtained from the correlation recommended by the textbook of Kreith and Bohn [16] is about 13% for $S \geqslant 0.008$ m or $Ra_s \geqslant 93.659$. However, their variation can be up to 45% for $S = 0.005$ m. This implies that the radiation heat transfer may be quite significant in natural convection for the smaller fin spacing. The similar result can also be found from Ref. [4].

Once the average heat transfer coefficient on each sub-fin region can be obtained, the temperature distribution on the whole annular circular fin can also be determined from Eq. (13). However, it should be noted that the average heat transfer coefficient on each sub-fin region is the approximate value. Thus the distribution of the calculated temperature on the whole annular circular fin is also an approximate contour for various S values. Figs. 9–11 show the distributions of the calculated temperature on the whole annular circular fin for various S values. It can be observed from Figs. 9–11 that, due to the poor thermal conductivity of the stainless fin, there is a considerable temperature drop between the tube wall and the edge of the annular circular fin. The fin temperature distributions obviously depart from the ideal isothermal situation and the fin temperature decreases more rapidly away from the circular center for larger values of the fin spacing.

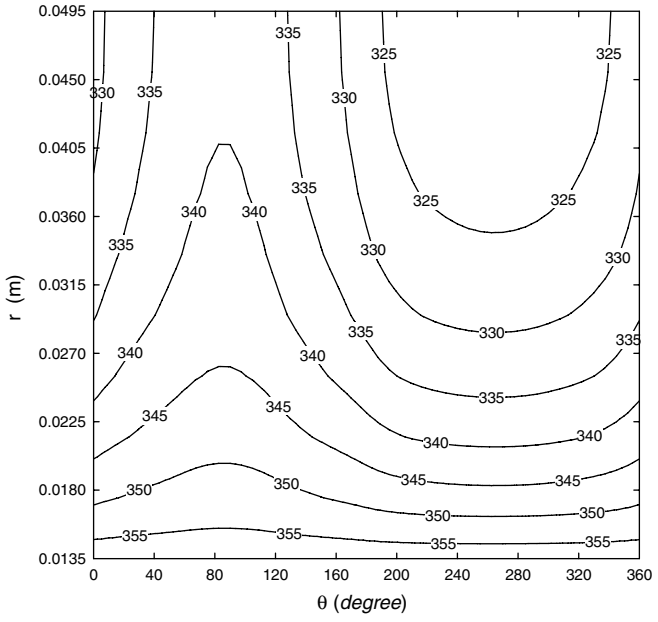

Fig. 9. Distribution of the calculated fin temperature for $S = 0.005$ m.

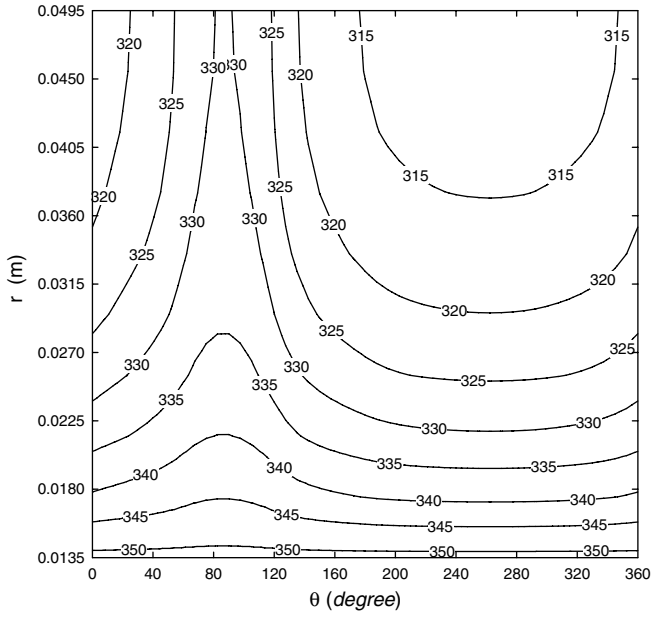

Fig. 10. Distribution of the calculated fin temperature for $S = 0.01$ m.

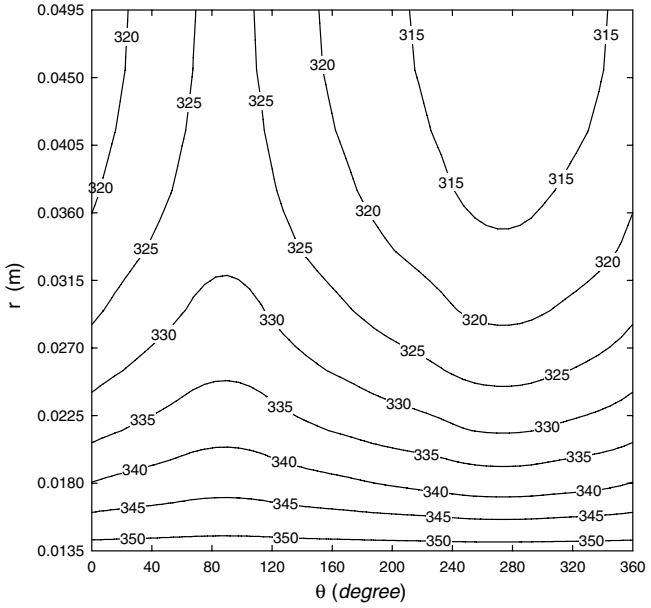

Fig. 11. Distribution of the calculated fin temperature for $S = 0.02$ m.

6. Conclusions

The present study proposes a numerical inverse scheme involving the finite difference method in conjunction with the least-squares method and experimental fin temperatures at six measurement locations to estimate the average heat transfer coefficient on the whole plate fin $\bar{h}$ and fin efficiency η_f in natural convection for various T_o, T_∞ and S values. The estimated results show that the fin temperature distributions depart from the ideal isothermal situation and the fin temperature decreases more rapidly away from the circular center when the fin spacing increases. The $\bar{h}$ value increases with increasing the fin spacing S. However, the η_f value decreases with increasing the S value. Variations of the $\bar{h}$ and η_f values with the S value approach their corresponding asymptotical values obtained from a single annular circular fin as $S \to \infty$. The present estimates can be obtained over a reasonably wide range of fin spacings. In general, the deviation of the $\bar{h}$ value between the present estimates under the ideal isothermal situation and the empirical values obtained from the correlation recom-

mended by the textbook of Kreith and Bohn [16] is about 13% for $S \geqslant 0.008$ m. However, their variation can be up to 45% for $S = 0.005$ m. This implies that the radiation heat transfer may be quite significant in natural convection for the smaller fin spacing.

Acknowledgements

The authors gratefully acknowledge the financial support provided by the National Science Council of the Republic of China under Grant No. NSC 92–2622–E006–146.

References

[1] G.D. Raithby, K.G.T. Hollands, Natural convection, in: W.M. Rohsenow, J.P. Hartnett, E.N. Ganic (Eds.), Handbook of Heat Transfer Fundamentals, second ed., McGraw-Hill, New York, 1985.
[2] J.L. Lage, Tube-to-tube heat transfer degradation effect on finned-tube heat exchangers, Numer. Heat Transfer A 39 (2001) 321–337.
[3] H.T. Chen, J.P. Song, Y.T. Wang, Prediction of heat transfer coefficient on the fin inside one-tube plate finned-tube heat exchangers, Int. J. Heat Mass Transfer 48 (2005) 2697–2707.
[4] H.T. Chen, J.C. Chou, Investigation of natural-convection heat transfer coefficient on a vertical square fin of finned-tube heat exchangers, Int. J. Heat Mass Transfer 49 (2006) 3034–3044.
[5] R.L. Webb, Principles of Enhanced Heat Transfer, Wiley, New York, 1994, pp. 125–153.
[6] Ş. Yildiz, H. Yüncü, An experimental investigation on performance of annular fins on a horizontal cylinder in free convection heat transfer, Heat Mass Transfer 40 (2004) 239–251.
[7] M.N. Özisik, Heat Conduction, second ed., Wiley, New York, 1993, Chapter 14.
[8] K. Kurpisz, A.J. Nowak, Inverse Thermal Problems, Computational Mechanics Publications, Southampton, UK, 1995.
[9] J. H Lin, C.K. Chen, Y.T. Yang, An inverse estimation of the thermal boundary behavior of a heated cylinder normal to a laminar air stream, Int. J. Heat Mass Transfer 43 (2000) 3991–4001.
[10] F.E.M. Saboya, E.M. Sparrow, Local and average heat transfer coefficients for one-row plate fin and tube heat exchanger configurations, ASME J. Heat Transfer 96 (1974) 265–272.
[11] E.C. Rosman, P. Carajilescov, F.E.M. Saboya, Performance of one- and two-row tube and plate fin heat exchangers, ASME J. Heat Transfer 106 (1984) 627–632.
[12] H. Ay, J.Y. Jang, J.N. Yeh, Local heat transfer measurements of plate finned-tube heat exchangers by infrared thermography, Int. J. Heat Mass Transfer 45 (2002) 4069–4078.
[13] K. Park, D.H. Choi, K.S. Lee, Optimum design of plate heat exchanger with staggered pin arrays, Numer. Heat Transfer A 45 (2004) 347–361.
[14] S.W. Churchill, H.H.S. Chu, Correlating equations for laminar and turbulent free convection from horizontal cylinder, Int. J. Heat Mass Transfer 18 (1975) 1049–1053.
[15] V.T. Morgan, The overall convective heat transfer from smooth circular cylinder, in: T.F. Irvine, J.P. Harnett (Eds.), Adv. Heat Transfer, vol. 11, Academic Press, New York, 1975, pp. 199–264.
[16] F. Kreith, M.S. Bohn, Principles of Heat Transfer, fifth ed., West Publishing Co., New York, 1993.
[17] A. Bejan, Heat Transfer, John Wiley and Sons, Inc., New York, 1993, pp. 53–62.
[18] V.S. Arpaci, S.H. Kao, A. Selamet, Introduction to Heat Transfer, Prentice-Hall, NJ, 1999, pp. 202–205.
[19] C.D. Jones, L.F. Smith, Optimum arrangement of rectangular fins on horizontal surfaces for free convection heat transfer, ASME J. Heat Transfer 92 (1970) 6–10.